Original Article

Improved detection of solitary pulmonary nodules on radiographs compared with deep bone suppression imaging

Jiefang Wu[1#], Weiguo Chen[1#], Fengxia Zeng[1], Le Ma[1], Weimin Xu[1], Wei Yang[2], Genggeng Qin[1]

[1]Department of Radiology, Nanfang Hospital, Southern Medical University, Guangzhou, China; [2]School of Biomedical Engineering, Southern Medical University, Guangzhou, China

Contributions: Conception and design: J Wu, W Yang, G Qin; (II) Administrative support: W Chen, G Qin; (III) Provision of study materials or patients: J Wu, L Ma; (IV) Collection and assembly of data: J Wu, W Xu; (V) Data analysis and interpretation: J Wu, F Zeng; (VI) Manuscript writing: all authors; (VII) Final approval of manuscript: all authors.

[#]These authors contributed equally to this work.

Correspondence to: Genggeng Qin. Department of Radiology, Nanfang Hospital, Southern Medical University, 1838 Guangzhou Avenue North, Baiyun District, Guangzhou, China. Email: 1425221889@qq.com and zealotq@smu.edu.cn.

Background: The present study aimed to investigate whether deep bone suppression imaging (BSI) could increase the diagnostic performance for solitary pulmonary nodule detection compared with digital tomosynthesis (DTS), dual-energy subtraction (DES) radiography, and conventional chest radiography (CCR).

Methods: A total of 256 patients (123 with a solitary pulmonary nodule, 133 with normal findings) were included in the study. The confidence score of 6 observers determined the presence or absence of pulmonary nodules in each patient. These were first analyzed using a CCR image, then with CCR plus deep BSI, then with CCR plus DES radiography, and finally with DTS images. Receiver-operating characteristic curves were used to evaluate the performance of the 6 observers in the detection of pulmonary nodules.

Results: For the 6 observers, the average area under the curve improved significantly from 0.717 with CCR to 0.848 with CCR plus deep BSI (P<0.01), 0.834 with CCR plus DES radiography (P<0.01), and 0.939 with DTS (P<0.01). Comparisons between CCR and CCR plus deep BSI found that the sensitivities of the assessments by the 3 residents increased from 53.2% to 69.5% (P=0.014) for nodules located in the upper lung field, from 30.6% to 44.6% (P=0.015) for nodules that were partially/completely obscured by the bone, and from 33.2% to 45.8% (P=0.006) for nodules <10 mm.

Conclusions: The deep BSI technique can significantly increase the sensitivity of radiology residents for solitary pulmonary nodules compared with CCR. Increased detection was seen mainly for smaller nodules, nodules with partial/complete obscuration, and nodules located in the upper lung field.

Keywords: Bone suppression; solitary pulmonary nodules; dual-energy subtraction; digital tomosynthesis

Submitted Dec 09, 2020. Accepted for publication May 18, 2021.
doi: 10.21037/qims-20-1346
View this article at: https://dx.doi.org/10.21037/qims-20-1346

Introduction

Conventional chest radiography (CCR) is widely used in the initial examination of any chest-related signs and symptoms, such as pulmonary cavities and pulmonary nodules, especially in developing countries. However, this has resulted in a higher false-negative rate of pulmonary nodules on chest radiographs, especially among the less experienced radiologists. Lung nodules obscured by bone structures represent a common contributor to misdiagnosis, especially nodules with a diameter <10 mm (1).

Some advanced imaging techniques are capable of decreasing or completely removing the over projection of the clavicles and ribs, such as dual-energy subtraction (DES) radiography, bone suppression imaging (BSI), and digital tomosynthesis (DTS). These techniques can improve the visibility of pulmonary nodules, increasing their detection rate (2-4). DES can produce tissue- and bone-selective images using low- and high-energy acquisitions from X-ray projections. DTS provides a series of thin-section reconstructed images at multiple angles (5,6). However, DES and DTS require special equipment and involve high radiation doses when used for nodule detection (7).

As a software product, BSI was developed to suppress bone structures, such as the ribs and clavicles, in the original chest images without the need for special hardware or increasing patients' doses due to slightly more prolonged exposure (8,9). Multiple studies have shown that the addition of BSI improves the detection rates of pulmonary nodules and reduces the false-positive findings with chest radiographs (3,4,10).

However, the large-scale application of BSI techniques is limited by the tedious training process, time-consuming image processing, and occasionally unstable outcomes. Therefore, a new bone suppression technology, deep BSI, was developed by our scientific research team. The deep BSI model is a 4-level cascade of multiscale ConvNets in a gradient-domain that can be refined to predict bone gradients. The bone gradients that the cascade model predicted at different scales were merged into a maximum-a-posteriori framework to produce the final estimation of a bone image. This final estimation of a bone image was suppressed from the chest image to produce a single soft-tissue image. We finally obtained 3 images. These were the original chest image, a single bone image, and a single soft-tissue image. Each ConvNet in the cascade model comprises 3 convolution layers with kernel sizes of 16×16, 1×1, and 8×8 and a channel number of 256. Mirror reflection padding was used to create equal input and output sizes (11).

There are differences between the deep BSI and other bone suppression techniques. First, the cascade architecture ensures that the receptive field of the CamsNet is large enough to extract and predict the corresponding bone composition information. Second, the convolutional neural networks (ConvNets) for different scales are trained to learn the mappings between original images and their bone components in the gradient domain. Separating the soft-tissue and bone components of original images was more accessible in the gradient domain than in the intensity domain. Third, compared with previous models of bone suppression, our models were based on training a large number of DES images (404 cases). For example, there were only 5 training cases in (12). In addition, our model did not require complicated contrast normalization procedures or the segmentation of the lung field for the original input images. Finally, the fusion of multiscale bone gradients in the MAP framework for bone image estimation can provide predictive information and further improve the quality of the estimated bone images.

The present study aimed to investigate whether deep BSI combined with a CCR image can improve an observer's performance in detecting pulmonary nodules in a multireader study by comparing its diagnostic value with those of DTS, CCR plus DES, and CCR.

Methods

The study was conducted following the Declaration of Helsinki (as revised in 2013). The Ethics Committee approved this retrospective study of Nanfang Hospital, Southern Medical University, and individual consent for this retrospective analysis was waived.

Study population

The study was conducted between December 2016 and September 2017 at Nanfang Hospital, Southern Medical University, Guangzhou, China. A total of 3,000 inpatients and outpatients were screened, all of whom underwent chest radiographs, and chest computed tomography (CT) scans within 3 months. All the diagnoses were confirmed with CT results. Lung nodule subtlety was classified into 5 categories by 2 chest radiologists (with 16 and 20 years of clinical experience, respectively), independently based on standard posterior–anterior (PA) chest radiography: 1, very subtle (average diameter: <3 mm); 2, subtle (<10 mm); 3, relatively subtle (>20 mm); and 4, obvious (<30 mm). The exclusion criteria were as follows: (I) very subtle nodules; (II) >2 nodules; (III) lung diseases that would affect the observation process, such as chronic bronchitis and massive pleural effusion; and (IV) poor image quality. The diameter of pulmonary nodules, defined as the mean of the shortest and longest diameters, was measured using CT images by another radiologist (with 10 years of experience). The 3 radiologists did not participate in the subsequent observer study.

Finally, a total of 256 patients were screened. Of these,

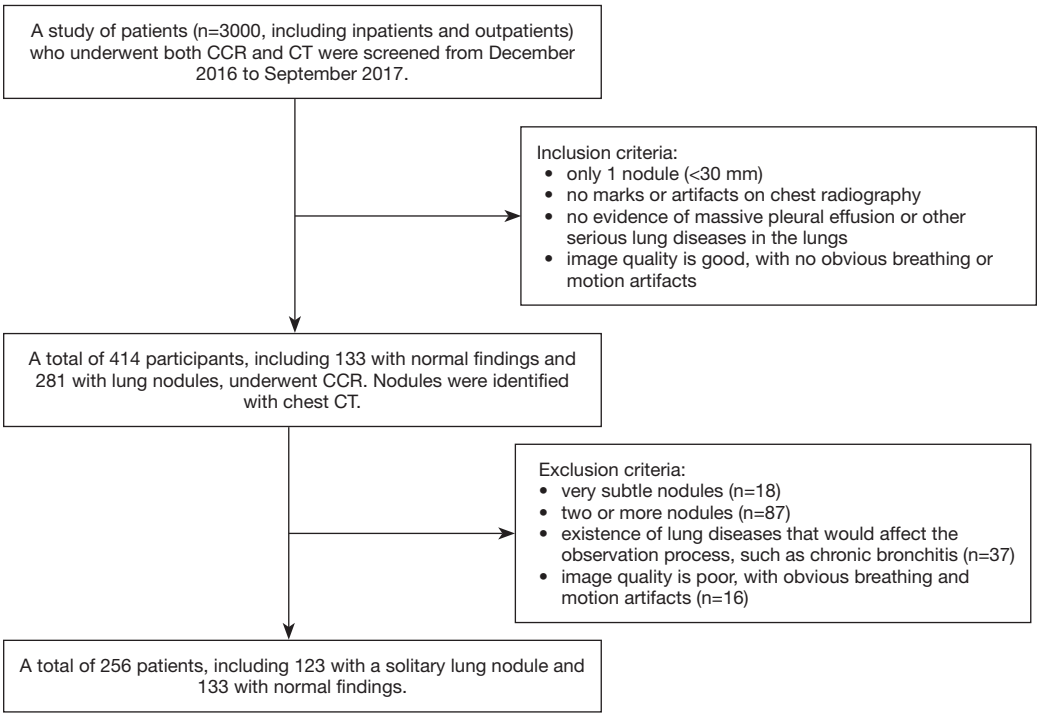

Figure 1 Flowchart of inclusion and exclusion criteria. CCR, conventional chest radiography; CT, computed tomography.

123 patients (average age: 42.4 years, range: 18–70 years), comprising 54 women and 79 men, had solitary lung nodules, and 133 patients (average age: 52.1 years, range: 18–79 years), comprising 40 women and 83 men had normal findings (*Figure 1*).

Image acquisition

A digital chest system (Discovery XR656; GE Healthcare, Madison, Wisconsin, USA) was used to obtain the CCR, DES, and DTS images within 3 months. The GE digital detector is a single panel (non-tiled) amorphous silicon detector with a cesium iodide scintillator. The detector has an active detector area of 41×41 cm, a matrix of 2022×2022 elements, 200 μm pixel size, and a 14-bit digitization depth. A chest PA view was obtained with automatic exposure control, for which the tube voltage was set as 120 kVp, the tube current was 500 mA, and the source to image distance was 180 cm. The DES images were obtained using a double-exposure technique between the high-energy (120 kV) and low-energy (60 kV) exposures. The DTS images were collected with a tube sweep angle of approximately ±15°and within 10 s, and with a fixed detector position. Fifty-three coronal images were reconstructed at 5-mm intervals. The chest CT images were collected using a 128-bit CT system (Brilliance ict 256; Philips Medical Systems, Amsterdam, the Netherlands), and the processing parameters were as follows: detector collimation, 64×0.625 mm; pitch, 0.673; rotation time, 0.5 s; and tube voltage, 120 kVp. The reconstruction section thickness for all patients was 5 mm.

The deep BSI model is the only self-developed bone suppression technology in China and has a national invention patent (X-ray chest bone suppression treatment method based on a ConvNet, China, 201510818953.3). The detailed model training process is shown in *Figure 2*.

The 5 modality images were CCRs, deep BSI, DES, DTS, and CT, and their pixel sizes were 0.194 mm, 0.194 mm, 0.194 mm, 0.20 mm, and 0.976 mm, respectively.

Image analysis

Of the 123 lung nodules, 35 were in the upper lung field, 49 in the middle lung field, and 39 in the lower lung field. Among all nodules, 73 were <10 mm in diameter, and 50 were 10–30 mm. The degree of overlap of bone structures was divided into 2 types by the researcher: minimal (<50%

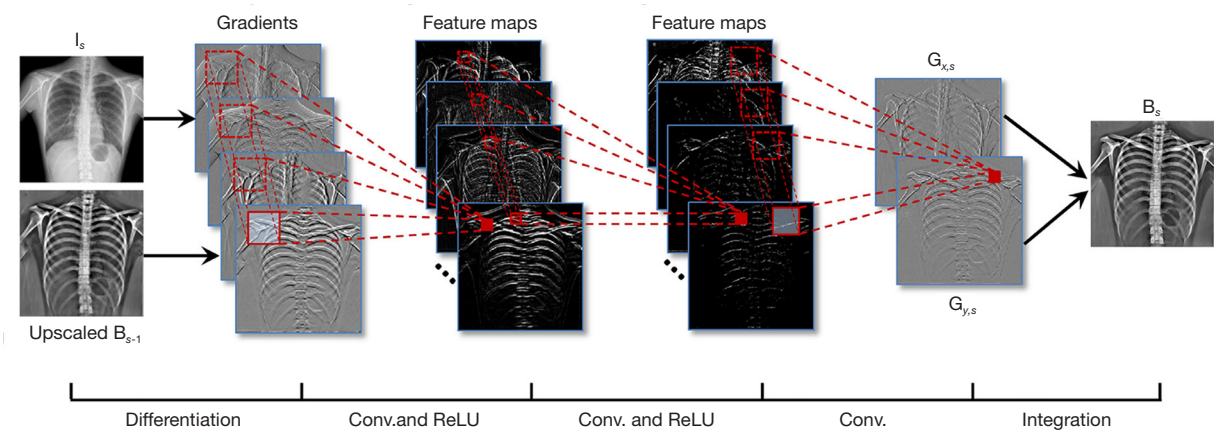

Figure 2 Technical route of deep bone suppression imaging (deep BSI) software. Basic prediction pipeline of bone images using deep convolutional neural network (ConvNet). Gradients of the downscaled input conventional chest radiography (I*s*) and the upscaled bone image (Bs_{-1}) were predicted by a unit for a coarse scale as the input feature maps of the ConvNet. Predicted gradients of the bone image at a finer scale as the outputs of the ConvNet, which were integrated to reconstruct the bone image B*s*. conv. = convolutional neural network. ReLU = rectified linear unit. I is an input CXR. G is a gradient image. B*s* is the predicted bone image at scale $1/2^{S-s}$ (s = 1, 2,…, S). S is the level number of the cascade. x and y is the horizontal and vertical gradients.

Table 1 Patient demographics and single nodule baseline characteristics (n=123)

Cases	Average diameter (mm)	Proportion (%)
Total (n=123)	12.89±0.62	
Male	14.05±0.83	67% (83/123)
Female	10.47±0.82	33% (40/123)
Location		
Upper	13.25±1.36	28% (35/123)
Middle	10.99±0.90	40% (49/123)
Lower	14.14±0.99	32% (39/123)
Nodule diameter (mm)		
<10	5.47±0.14	59% (72/123)
>10	23.36±1.01	41% (51/123)
Overlapping bone structures		
<50%	10.63±0.43	59% (73/123)
>50%	11.18±0.90	41% (50/123)

Nodules were divided into the following 2 groups, according to the area of overlap with bone structures: minimal overlap area (<50%) and partial/complete overlap area (>50%).

of the nodule area) and partial/complete (50–100%) (*Table 1*).

Six observers, comprising 3 radiologists (10–30 years' experience each) and 3 radiology residents (2–3 years' experience each), evaluated the 256 study cases in different randomized orders. All the observers were unaware of the patients' clinical profiles and did not know the number and position of the nodules and CT findings. Six 3-megapixel medical liquid crystal display monitors (RadiForce GS320; Eizo, Ishikawa, Japan) were used in the observer study. The monitors had a screen size of 21.3 inches and a screen resolution of 2048×1536. All the observers were allowed to change the window width and window level, invert grayscale or zoom in/out images at their discretion. The observers underwent training on another set of deep BSI using images from 20 clinical cases before reading the images in the study group.

In each reading session, the observers first analyzed the CCR images, then CCR plus deep BSI images, then CCR plus DES images, and finally, the DTS images, with the reading time limited to 3 min. The following 4 groups of images were included in each reading task: CCR, CCR plus deep BSI, CCR plus DES, and DTS. These were arranged randomly and combined to ensure that the 4 groups of

Table 2 Area under the receiver-operating characteristic curve values in detecting pulmonary nodules for all observers in the 4 methods

	CCR	CCR+DES	CCR+Deep BSI	DTS
1	0.702	0.732	0.812	0.828
2	0.710	0.787	0.794	0.928
3	0.692	0.822	0.822	0.958
Radiology residents	0.700 (0.062, 0.737)	0.779 (0.745, 0.813)	0.810 (0.778, 0.842)	0.906 (0.883, 0.930)
4	0.728	0.882	0.866	0.947
5	0.742	0.885	0.884	0.971
6	0.736	0.896	0.913	0.988
Radiologists	0.735 (0.698, 0.770)	0.888 (0.862, 0.914)	0.887 (0.861, 0.912)	0.969 (0.955, 0.983)
All observers	0.717 (0.691, 0.743)	0.834 (0.812, 0.855)	0.848 (0.827, 0.868)	0.939 (0.925, 0.952)

Unless otherwise indicated, data are areas under the curve. For radiologists with different clinical experiences, the differences were statistically significant between conventional chest radiography (CCR) and the other 3 methods (P<0.05). For all observers, there was no statistical significance between conventional chest radiography plus dual-energy subtraction (DES) and conventional chest radiography plus deep bone suppression imaging (deep BSI) (P=0.213). Results are the same for the 3 radiology residents (P=0.801) and 3 radiologists (P=0.120). DTS, digital tomosynthesis.

images were from different patients.

The observers were requested to identify patients with pulmonary nodules and identify the location of the nodules. The observers scored suspicious nodules for each image using a continuous score between 0 and 100 (0=not suspicious, 100=definitely suspicious). The larger the value, the greater the possibility of a suspected nodule. In this test, after moving on to the following images, the observers could not change the position and score of the nodule of the previous image.

Statistical analysis

The observer performance was analyzed using a multiple-reader, multiple-case receiver-operating characteristic (ROC) method, assigning the score of the most suspicious finding to each case. A computer program (MRMCaov R package, https://pubmed.ncbi.nlm.nih.gov/32351258) that included case and reader into the analysis was used to test the differences in the observer's performance. The bi-normal ROC curves were obtained from the ordinal-scale rating data using this program. The area under the ROC curve was compared for all nodules and nodular subgroups according to nodule characteristics and the degree of bone overlap.

We calculated the overall sensitivity and specificity of the observer, taking the results with scores >50 into account. The sensitivities of the 4 techniques were compared with each other using a non-parametric test (SPSS version 17.0; SPSS, Chicago, IL, USA), with P<0.05 indicating statistical significance.

Results

Observer performance: ROC analysis

The average areas under the curve (AUCs) improved significantly for all the observers, from 0.717 with CCR alone to 0.848 with CCR+deep BSI, 0.834 with CCR+DES, and 0.939 with DTS. The average AUCs for the 3 residents were 0.700 with CCR alone, 0.810 with CCR+deep BSI, 0.779 with CCR+DES, and 0.906 with DTS. The average AUCs for the 3 radiologists were 0.735 with CCR alone, 0.887 with CCR+deep BSI, 0.888 with CCR+DES, and 0.969 with DTS (*Table 2* and *Figure 3*).

Observer performance: sensitivity and specificity

For all the observers, the diagnostic sensitivities of CCR, CCR+DES, CCR+deep BSI, and DTS were 53.8% (397/738), 70% (516/738), 67.1% (495/738), and 84.6% (624/738), respectively. For the 3 radiologists, the sensitivities were 55.8% (206/369), 79.4% (292/369), 76.9% (284/369), and 89.9% (331/369), respectively. For the residents, the sensitivities were 50.9% (188/369), 60.9% (225/369), 60.4% (223/369), and 80.5% (297/369), respectively. For all the observers, the specificities of CCR, CCR+DES, CCR+deep BSI, and DTS were 83.7% (668/798), 90.1% (719/798), 89.6% (715/798), and 95.7% (764/798), respectively. For the 3 radiologists, the specificities were 83.9% (309/369), 91.7% (338/369),

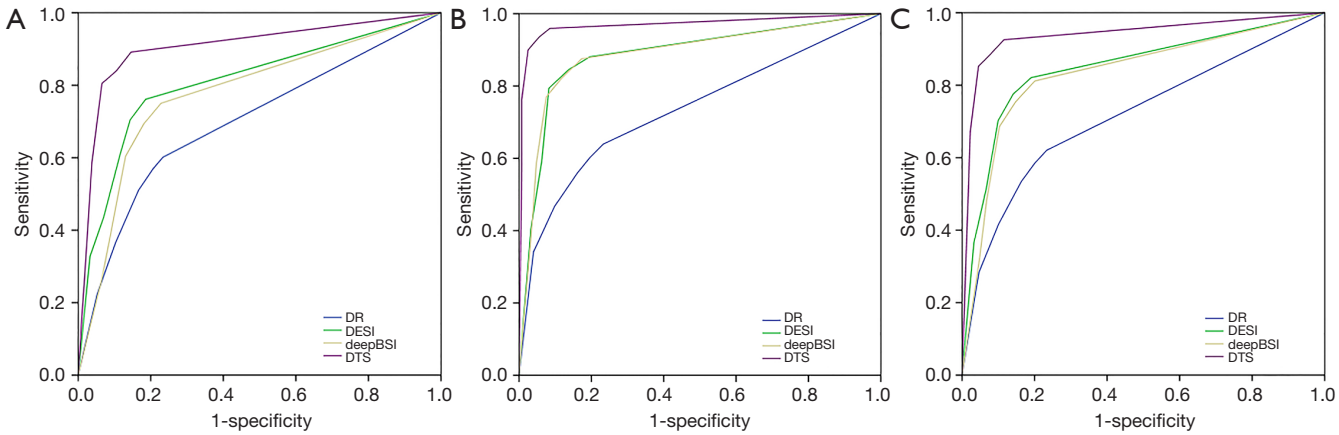

Figure 3 Receiver-operating characteristic (ROC) curves of all observers' performance for conventional chest radiography (CCR), conventional chest radiography plus deep bone suppression imaging (deep BSI), conventional chest radiography plus dual-energy subtraction (DES), and digital tomosynthesis (DTS). (A) Graphs show ROC curves for the detection of solitary pulmonary nodules by 3 radiology residents. Differences in areas under the curve (AUCs) were statistically significant between CCR and CCR+DES, between CCR and CCR+deep BSI, and between CCR and DTS (P<0.05). (B) Graphs show ROC curves for the detection of solitary pulmonary nodules by 3 radiologists. Differences in AUCs between CCR and CCR+DES, between CCR and CCR+deep BSI, and between CCR and DTS were statistically significant (P<0.05). (C) ROC curves for the detection of solitary pulmonary nodules by all observers. Differences in AUCs between CCR and CCR+DES, between CCR and CCR+deep BSI, and between CCR and DTS were statistically significant (P<0.05).

92.4% (341/369), and 97.4% (359/369), respectively. For the 3 residents, the specificity were 83.4% (308/369), 88.4% (326/369), 86.7% (320/369), and 93.4% (345/369), respectively.

Performance for different nodule types

For the nodules located in the upper lung field, the sensitivities of assessments by the 3 residents increased from 53.2% with CCR alone to 69.5% with CCR+deep BSI (P=0.014). For the nodules in the middle lung field, the sensitivity of CCR+deep BSI (61.9%) was higher than that of CCR (53.7%, P=0.081). For nodules in the lower lung field, the sensitivity of CCR+deep BSI was 50.4% compared with that of CCR, which was 43.5% (P=0.291).

In the assessment by the 3 residents showing nodules that were partially/completely obscured by bone, the average sensitivity increased from 30.6% with CCR alone to 44.6% (P=0.015) with CCR+deep BSI, and the sensitivity of CCR was 63.5%, while the sensitivity of CCR+deep BSI was 71.2% (P=0.053) for nodules that were minimally obscured by bone.

In comparisons between CCR and CCR+deep BSI, the sensitivity of assessments by the 3 residents increased from 33.2% to 45.8% (P=0.006) for smaller nodules, with the sensitivity of CCR+deep BSI (81%) being higher than that of CCR (74.5%, P=0.174) for the larger nodules (*Table 3*).

The deep BSI and DES techniques consistently achieved similar sensitivities (P=0.05). These results are summarized in *Table 4*.

The mean effective doses of CCR, CCR+DES, DTS, and CT were 0.04 mSv (range: 0.03–0.14 mSv), 0.067 mSv (range: 0.044–0.16 mSv), 0.107 mSv (range: 0.094–0.22 mSv), and 6.8 mSv (range: 3.9–12 mSv), respectively. As a computer post-processing software, CCR+deep BSI did not increase patients' radiation doses compared with CCR.

Discussion

Failure to detect nodules on chest radiography was due in part to the superimposition of lesions on other structures, such as the diaphragm, mediastinum, heart, clavicles, ribs, and pulmonary vessels, and to the size and location of the nodule. Using DES and DTS techniques and a post-processing BSI algorithm can suppress the conspicuity of bones (*Figure 4*). However, the disadvantages of DES and DTS radiography include the need for specialized equipment, increased cost, and slightly longer examination times, which was prone to breathing and motion artifacts and potential increases in radiation dose.

Previously published studies have confirmed that bone

Table 3 Sensitivities of the 4 methods for the identification of lung nodules for all observers

	Group	CCR	CCR+Deep BSI	P value	CCR	CCR+DES	P value	CCR	DTS	P value
Location										
Upper	A	53.2	69.5	0.014	53.2	67.6	0.008	53.2	82.8	0.000
	B	65.7	79.0	0.004	65.7	80.9	0.001	65.7	91.4	0.000
	C	60.4	74.3	0.000	60.4	74.2	0.000	60.4	87.1	0.000
Middle	A	53.7	61.9	0.081	53.7	62.5	0.016	53.7	82.3	0.000
	B	57.1	80.9	0.000	57.1	81.5	0.000	57.1	89.8	0.000
	C	55.4	71.4	0.000	55.4	71.7	0.000	55.4	86.0	0.000
Lower	A	43.5	50.4	0.291	43.5	52.9	0.061	43.5	76.0	0.000
	B	49.8	61.6	0.041	49.8	72.5	0.000	49.8	85.9	0.000
	C	44.4	59.8	0.000	44.4	64.5	0.000	44.4	82.4	0.000
Overlapping bone structures										
>50%	A	30.6	44.6	0.015	30.6	41.5	0.023	30.6	72.0	0.000
	B	34.0	56.8	0.000	34.0	64.0	0.000	34.0	85.3	0.000
	C	33.0	52.0	0.000	33.0	52.7	0.000	33.0	78.7	0.000
<50%	A	63.5	71.2	0.053	63.5	74.4	0.000	63.5	86.3	0.000
	B	72.5	85.0	0.000	72.5	88.6	0.000	72.5	91.3	0.000
	C	67.3	79.9	0.000	67.3	82.1	0.000	67.3	89.7	0.000
Nodule diameter (mm)										
<10	A	33.2	45.8	0.006	33.2	43.6	0.006	33.2	70.3	0.000
	B	38.4	62.0	0.000	38.4	66.2	0.000	38.4	83.8	0.000
	C	36.3	53.9	0.000	36.3	54.6	0.000	36.3	77.0	0.000
>10	A	74.5	81.0	0.174	74.5	86.2	0.001	74.5	94.3	0.000
	B	83.8	90.2	0.096	83.8	95.6	0.000	83.8	95.4	0.000
	C	79.8	85.7	0.094	79.8	91.2	0.000	79.8	94.8	0.000

Unless otherwise indicated, data are sensitivities. For nodules located in the upper lung field, the sensitivity of assessments by the 3 residents increased from 53.2% with conventional chest radiography (CCR) alone to 69.5% with conventional chest radiography plus deep bone suppression imaging (deep BSI) (P=0.014). Sensitivity did not reach statistical significance for nodules located in middle and lower lung fields (P=0.081 and P=0.291, respectively). For nodules that were partially/completely obscured by bone, sensitivity increased significantly between CCR and conventional chest radiography plus deep BSI (30.6% vs. 44.6%, P=0.015). Sensitivity increased from 33.2% to 45.8% (P=0.006) for smaller nodules. A, 3 residents; B, 3 radiologists; C, 6 observers. DES, dual-energy subtraction; DTS, digital tomosynthesis.

suppression techniques can have greater sensitivities than CCR (3,13,14). Schalekamp *et al*. reported that the sensitivity increased from 59.8% with CCR to 67.6% with CCR+BSI (P=0.002), whereas specificity decreased from 91% with CCR to 88.4% with CCR+BSI (P=0.07) (3).

In the present study, the performance was improved significantly (P<0.05) for smaller nodules (<10 mm) with the use of CCR+deep BSI for the 3 residents. Schalekamp *et al*. classified nodules into the following 4 categories, based on their visibility: from obvious to moderate, subtle (average diameter: >15 mm), and very subtle (average diameter: <15 mm). The increase in detection performance using CCR+BSI was the highest for subtle nodules (P=0.03), while this difference did not reach statistical significance

Table 4 Sensitivities of the 4 methods for the identification of lung nodules for all observers

	Group	CCR+deep BSI	DTS	P value	CCR+DES	DTS	P value	CCR+deep BSI	CCR+DES	P value
Location										
Upper	A	69.5	82.8	0.016	67.6	82.8	0.005	69.5	67.6	0.367
	B	79.0	91.4	0.011	80.9	91.4	0.031	79.0	80.9	0.225
	C	74.3	87.1	0.000	74.2	87.1	0.000	74.3	74.2	0.924
Middle	A	61.9	82.3	0.000	62.5	82.3	0.000	61.9	62.5	0.490
	B	80.9	89.8	0.009	81.5	89.8	0.008	80.9	81.5	0.214
	C	71.4	86.0	0.000	71.7	86.0	0.000	71.4	71.7	0.818
Lower	A	50.4	76.0	0.000	52.9	76.0	0.000	50.4	52.9	0.415
	B	61.6	85.9	0.000	72.5	85.9	0.020	61.6	72.5	0.109
	C	59.8	82.4	0.000	64.5	82.4	0.000	59.8	64.5	0.627
Overlapping bone structures										
>50%	A	44.6	72.0	0.000	41.5	72.0	0.000	44.6	41.5	0.964
	B	56.8	85.3	0.000	64.0	85.3	0.000	56.8	64.0	0.123
	C	52.0	78.7	0.000	52.7	78.7	0.000	52.0	52.7	0.313
<50%	A	71.2	86.3	0.000	74.4	86.3	0.001	71.2	74.4	0.341
	B	85.0	91.3	0.038	88.6	91.3	0.362	85.0	88.6	0.203
	C	79.9	89.7	0.000	82.1	89.7	0.000	79.9	82.1	0.929
Nodule diameter (mm)										
<10	A	45.8	70.3	0.000	43.6	70.3	0.000	45.8	43.6	0.888
	B	62.0	83.8	0.000	66.2	83.8	0.000	62.0	66.2	0.322
	C	53.9	77.0	0.000	54.6	77.0	0.000	53.9	54.6	0.426
>10	A	81.0	94.3	0.000	86.2	94.3	0.019	81.0	86.2	0.318
	B	90.2	95.4	0.096	95.6	95.4	0.098	90.2	95.6	0.078
	C	85.7	94.8	0.000	91.2	94.8	0.096	85.7	91.2	0.720

Unless otherwise indicated, data are sensitivities. Conventional chest radiography plus deep bone suppression imaging (deep BSI) and conventional chest radiography plus dual-energy subtraction (DES) had similar sensitivity (P>0.05). For nodules that were minimally obscured by bone, the average sensitivity increased from 85% with CCR+deep BSI to 91.3% (P=0.038) with digital tomosynthesis (DTS) by radiologists, and sensitivity increased from 90.2% to 95.4% (P=0.096) for larger nodules. A, 3 residents; B, 3 radiologists; C, 6 observers.

for very subtle nodules (P=0.11). The detection of nodules <3 mm, which were not analyzed in the present study, remains a problem with projection radiography, even with the concurrent application of various enhancing techniques. When detected incidentally, small lesions may not present an immediate risk to the patient; they can change diagnostic or therapeutic decisions in patients with known primary malignancy. To date, these diagnostic problems can best be solved by CT.

In our daily clinical routine, these types of lesions are mostly partial/complete obscuration or located in the upper lung fields, particularly prone to the inattentional blindness of the observers, especially inexperienced observers. Therefore, the finding that deep BSI increased the detection rates of these types of lung nodules, leading to improved observer performance, is essential. This result was consistent with those from other studies that showed that CCR+DES and CCR+BSI were beneficial for inexperienced readers. However, their improved sensitivities in lung nodule detection came at the cost of reduced specificities

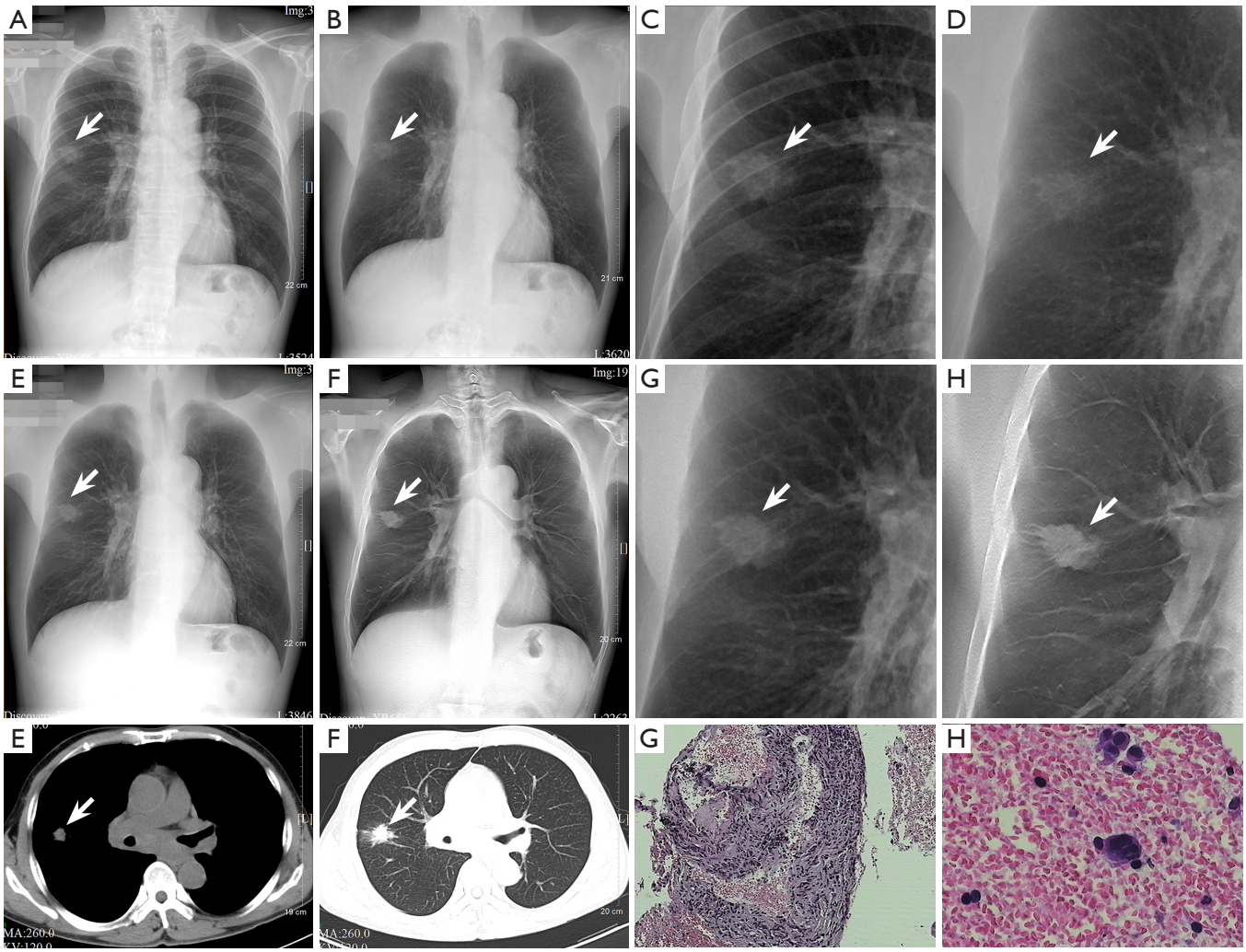

Figure 4 Images of a 53-year-old man with lung cancer in the right upper lung field. (A,C) Conventional chest radiography images show cancer partly obscured by ribs. (B,D) Deep bone suppression imaging of soft tissues clearly show the cancer location, with different lengths of burrs. (E,G) Dual-energy subtraction soft-tissue images also clearly show cancer. (F,H) Lesion features are apparent on digital tomosynthesis images, and even include pleural traction signs. (I,J) Computed tomography images show the nodule more details, with shallow lobulation, different lengths burrs, and pleural stretch. (K,L) Cellular immunohistochemistry results display creatine kinase (CK)(+) and CK5/6(+), and liquid-based cytology revealed atypical-shaped cells. Hematoxylin-eosin staining shows large and hyperchromatic nuclei with many mitotic images, and the pathological results indicated squamous cell carcinoma. The image indicated by the arrow represents pulmonary nodules. Magnification: G, 20, H, 400.

(4,15). Szucs-Farkas *et al*. reported that the increased sensitivity of BSI images compared with original chest radiographs was predominantly from the residents. In contrast, the expert radiologists increased their numbers of true positives by no more than 5% (4).

Compared with the findings of previously published studies, our study has several advantages. First, using CCR+deep BSI, we analyzed in detail the type of nodules, including the size, location, and degree of osseous superprojection. Second, the sensitivity of the CCR+deep BSI increased to 67.1% without a significant overall loss of specificity compared with CCR alone. Third, we used a new type of self-developed bone suppression software.

In addition, the findings of the present study indicated that CCR+deep BSI had a similar performance to CCR+DES. Li *et al*. found that while CCR+BSI improved

the accuracy of radiologists in detecting small lung cancers, CCR+DES provided even further improvements (16). To our knowledge, the present study was the first to compare BSI technology with DTS, CCR+deep BSI, and the DTS, with similar detection rates for larger pulmonary nodules (average diameter: >10 mm) among the 3 radiologists (P=0.096). This indicated that CCR+deep BSI could play an important role in clinical practice. DTS significantly improved the radiologists' detection performance for smaller nodules compared to CCR. This finding is supported by multiple studies and can be attributed to the multidimensional observation of lesions afforded by DTS (17-19). However, the operation time in DTS is more prolonged, making it more susceptible to breathing and heart movement than CCR+deep BSI. Therefore, lesions located in the hilar region, the shadow of the heart, and the mediastinum are easily missed (20).

Our study had several limitations. First, it was based on a relatively small sample size, and therefore, the prevalence of nodules may have been higher than the prevalence in clinical practice. Second, we did not compare deep BSI with conventional BSI because of the limitations in the conditions. This comparison will be addressed in our future studies. Previously published studies have indicated that low-dose computed tomography screening (LDCT) and computer-aided detection (CAD) have value in the diagnosis of pulmonary nodules, and we will compare CCR+deep BSI with LDCT and CAD in the diagnosis of pulmonary nodules in the future (21-24).

Furthermore, because we did not analyze the density of the nodules, the detection rates of different density nodules were not compared with the 4 methods. In our follow-up study, more cases will be analyzed. Finally, the experience levels of the readers were not homogeneous, and the observers were more familiar with CCR, CCR+DES, and DTS, but not with CCR+deep BSI. We provided a set of 20 cases to train observers, but more training may be necessary for a better understanding of the strengths and weaknesses of CCR+deep BSI.

Conclusions

The present study's findings indicated that CCR+deep BSI could improve the detection rates of lung nodules compared with the use of CCR alone. This was helpful to the residents, particularly to the radiology residents. The deep BSI techniques enabled the matching of different types of digital chest radiography techniques without the requirement of any special hardware or additional radiation doses. Therefore, deep BSI can reduce the financial burden and radiation doses of patients, particularly in developing countries, areas that do not have DES and DTS, and even in areas where it is difficult to perform CT.

Acknowledgments

Funding: This work was supported by the National Key Research and Development Project, China (Nos. 2019YFC0117300, 2019YFC0117301), the National Key Research and Development Project, China (Nos. 2019YFC0121900, 2019YFC0121903), the Natural Science Foundation of Guangdong Province, China (No. 2018A0303130215), the Natural Science Foundation of Guangdong Province, China (No. 2019A1515011168), and the Presidential Foundation of the Nanfang Hospital, Southern Medical University of Guangdong Province, China (No. 2018C015).

Footnote

Conflicts of Interest: All authors have completed the ICMJE uniform disclosure form (available at https://dx.doi.org/10.21037/qims-20-1346). The authors have no conflicts of interest to declare.

Ethical Statement: The authors are accountable for all aspects of the work in ensuring that questions related to the accuracy or integrity of any part of the work are appropriately investigated and resolved. The study was conducted in accordance with the Declaration of Helsinki (as revised in 2013). This retrospective study was approved by the Ethics Committee of Nanfang Hospital, Southern Medical University, and individual consent for this retrospective analysis was waived.

References

1. Oda S, Awai K, Funama Y, Utsunomiya D, Yanaga Y, Kawanaka K, Nakaura T, Hirai T, Murakami R, Nomori H, Yamashita Y. Detection of small pulmonary nodules on chest radiographs: efficacy of dual-energy subtraction technique using flat-panel detector chest radiography. Clin Radiol 2010;65:609-15.
2. Choo JY, Lee KY, Yu A, Kim JH, Lee SH, Choi JW, Kang EY, Oh YW. A comparison of digital tomosynthesis and chest radiography in evaluating airway lesions using computed tomography as a reference. Eur Radiol 2016;26:3147-54.
3. Schalekamp S, van Ginneken B, Meiss L, Peters-Bax L, Quekel LG, Snoeren MM, Tiehuis A M, Wittenberg R, Karssemeijer N, Schaefer-Prokop CM. Bone suppressed images improve radiologists' detection performance for pulmonary nodules in chest radiographs. Eur J Radiol 2013;82:2399-405.
4. Szucs-Farkas Z, Schick A, Cullmann JL, Ebner L, Megyeri B, Vock P, Christe A. Comparison of dual-energy subtraction and electronic bone suppression combined with computer-aided detection on chest radiographs: effect on human observers' performance in nodule detection. AJR Am J Roentgenol 2013;200:1006-13.
5. Vikgren J, Zachrisson S, Svalkvist A, Johnsson AA, Boijsen M, Flinck A, Kheddache S, Båth M. Comparison of chest tomosynthesis and chest radiography for detection of pulmonary nodules: human observer study of clinical cases. Radiology 2008;249:1034-41.
6. Dobbins JT 3rd, Godfrey DJ. Digital x-ray tomosynthesis: current state of the art and clinical potential. Phys Med Biol 2003;48:R65-106.
7. Dobbins JT 3rd, Mcadams HP, Sabol JM, Chakraborty DP, Kazerooni EA, Reddy GP, Vikgren J, Båth M. Multi-institutional evaluation of digital tomosynthesis, dual-energy radiography, and conventional chest radiography for the detection and management of pulmonary nodules. Radiology 2017;282:236-50.
8. Loog M, van Ginneken B, Schilham AM. Filter learning: application to suppression of bony structures from chest radiographs. Med Image Anal 2006;10:826-40.
9. von Berg J, Young S, Carolus H, Wolz R, Saalbach A, Hidalgo A, Giménez A, Franquet T. A novel bone suppression method that improves lung nodule detection: suppressing dedicated bone shadows in radiographs while preserving the remaining signal. Int J Comput Assist Radiol Surg 2016;11:641-55.
10. Li F, Hara T, Shiraishi J, Engelmann R, MacMahon H, Doi K. Improved detection of subtle lung nodules by use of chest radiographs with bone suppression imaging: receiver operating characteristic analysis with and without localization. AJR Am J Roentgenol 2011;196:W535-41.
11. Yang W, Chen Y, Liu Y, Zhong L, Qin G, Lu Z, Feng Q, Chen W. Cascade of multi-scale convolutional neural networks for bone suppression of chest radiographs in gradient domain. Med Image Anal 2017;35:421-33.
12. Suzuki K, Abe H, Macmahon H, Doi K. Image-processing technique for suppressing ribs in chest radiographs by means of massive training artificial neural network (MTANN). IEEE Trans Med Imaging 2006;25:406-16.
13. Freedman MT, Lo SC, Seibel JC, Bromley CM. Lung nodules: improved detection with software that suppresses the rib and clavicle on chest radiographs. Radiology 2011;260:265-73.
14. Schalekamp S, van Ginneken B, van den Berk IA, Hartmann IJ, Snoeren MM, Odink AE, van Lankeren W, Pegge SA, Schijf LJ, Karssemeijer N, Schaefer-Prokop CM. Bone suppression increases the visibility of invasive pulmonary aspergillosis in chest radiographs. PLoS One 2014;9:e108551.
15. Szucs-Farkas Z, Patak MA, Yuksel-Hatz S, Ruder T, Vock P. Single-exposure dual-energy subtraction chest radiography: detection of pulmonary nodules and masses in clinical practice. Eur Radiol 2008;18:24-31.
16. Li F, Engelmann R, Pesce LL, Doi K, Metz CE, Macmahon H. Small lung cancers: improved detection by use of bone suppression imaging--comparison with dual-energy subtraction chest radiography. Radiology 2011;261:937-49.
17. Kumar SG, Garg MK, Khandelwal N, Gupta P, Gupta D, Aggarwal AN, Bansal SC. Role of digital tomosynthesis and dual energy subtraction digital radiography in detecting pulmonary nodules. Eur J Radiol 2015;84:1383-91.
18. Gomi T, Nakajima M, Fujiwara H, Umeda T. Comparison of chest dual-energy subtraction digital tomosynthesis imaging and dual-energy subtraction radiography to detect simulated pulmonary nodules with and without calcifications a phantom study. Acad Radiol 2011;18:191-6.
19. Sharma M, Sandhu MS, Gorsi U, Gupta D, Khandelwal N. Role of digital tomosynthesis and dual energy subtraction digital radiography in detection of parenchymal lesions in active pulmonary tuberculosis. Eur J Radiol 2015;84:1820-7.
20. Galea A, Dubbins P, Riordan R, Adlan T, Roobottom C,

Gay D. The value of digital tomosynthesis of the chest as a problem-solving tool for suspected pulmonary nodules and hilar lesions detected on chest radiography. Eur J Radiol 2015;84:1012-8.
21. Aberle DR, Adams AM, Berg CD, Black WC, Clapp JD, Fagerstrom RM, Gareen IF, Gatsonis C, Marcus PM, Sicks JD. Reduced lung-cancer mortality with low-dose computed tomographic screening. N Engl J Med 2011;365:395-409.
22. Church TR, Black WC, Aberle DR, Berg CD, Clingan KL, Duan F, Fagerstrom RM, Gareen IF, Gierada DS, Jones GC, Mahon I, Marcus PM, Sicks JD, Jain A, Baum S. Results of initial low-dose computed tomographic screening for lung cancer. N Engl J Med 2013;368:1980-91.
23. Wang Z, Han W, Zhang W, Xue F, Wang Y, Hu Y, Wang L, Zhou C, Huang Y, Zhao S, Song W, Sui X, Shi R, Jiang J. Mortality outcomes of low-dose computed tomography screening for lung cancer in urban China: a decision analysis and implications for practice. Chin J Cancer 2017;36:57.
24. Novak RD, Novak NJ, Gilkeson R, Mansoori B, Aandal GE. A comparison of computer-aided detection (CAD) effectiveness in pulmonary nodule identification using different methods of bone suppression in chest radiographs. J Digit Imaging 2013;26:651-6.

Cite this article as: Wu J, Chen W, Zeng F, Ma L, Xu W, Yang W, Qin G. Improved detection of solitary pulmonary nodules on radiographs compared with deep bone suppression imaging. Quant Imaging Med Surg 2021;11(10):4342-4353. doi: 10.21037/qims-20-1346

